Sci. Dril., 33, 191–206, 2024
https://doi.org/10.5194/sd-33-191-2024

Scientific Drilling
Open Access

Shaped and filled by the Rhine Glacier: the overdeepened Tannwald Basin in southwestern Germany

Bennet Schuster[1,2,3], Lukas Gegg[1], Sebastian Schaller[2,3], Marius W. Buechi[2,3], David C. Tanner[4], Ulrike Wielandt-Schuster[5], Flavio S. Anselmetti[2,3], and Frank Preusser[1]

[1]Institute of Earth and Environmental Sciences, University of Freiburg, Albertstr. 23b, 79104 Freiburg, Germany
[2]Institute of Geological Sciences, University of Bern, Baltzerstr. 1+3, 3012 Bern, Switzerland
[3]Oeschger Centre for Climate Change Research, University of Bern, Hochschulstr. 4, 3012 Bern, Switzerland
[4]Leibniz Institute for Applied Geophysics, Stilleweg 2, 30655 Hannover, Germany
[5]Baden-Württemberg State Office for Geology, Mineral Resources, and Mining, Albertstraße 5, 79104 Freiburg, Germany

Correspondence: Bennet Schuster (bennet.schuster@geologie.uni-freiburg.de)

Received: 21 December 2023 – Revised: 5 May 2024 – Accepted: 15 May 2024 – Published: 4 July 2024

Abstract. The Alpine region was shaped by repeated glaciations during the Quaternary, which led to the formation of overdeepened valleys and basins. These features today, hidden below the present-day land surface, host multiple stacked and nested glacial sequences and offer valuable insight into the environmental history and geomorphological evolution of the region. The project Drilling Overdeepened Alpine Valleys (DOVE) of the International Continental Scientific Drilling Program (ICDP) is dedicated to investigating such overdeepened structures around the Alps. Within DOVE, we here focus on the Tannwald Basin in southern Germany. Situated distally within the area formerly occupied by the Rhine Glacier piedmont lobe; it was shaped by multiple glaciations, yet it is located outside the Last Glacial Maximum (LGM) ice extent. Previous seismic imaging and the presence of interglacial pollen sequences indicate a multi-phase infill history. The complex sedimentary architecture observed in a newly drilled core allows for comparison with seismic data and lithological evidence from other sites. On the basis of a lithofacies model that introduces 17 lithotypes, we propose that the basin fill is composed of three lithostratigraphic units that reflect the glacial history of the basin. After the erosion of the Tannwald Basin, a cold-climate, stacked basin-infill sequence recorded sedimentation of two glacial advances, before it was covered by LGM outwash. The sedimentary record includes an extensive basal glacial shear zone with deformed bedrock and several overlying diamict horizons. Further upcore, deformation structures underscore the role of gravitational processes as well as profound glaciotectonics, deforming the sediment deep within the subsurface. While the sedimentary record indicates a rather rapid infill of the depression, further age constraints and detailed investigations of ice-contact sediments will clarify open questions regarding the temporal classification of the deposits.

1 Introduction

The northern Alpine foreland witnessed repeated glacial cycles during the Quaternary period, comprising glacier expansion and decay (e.g., Doppler et al., 2011; Ellwanger et al., 2011; Preusser et al., 2011). By eroding and redepositing large rock and sediment masses, glaciers created landscape features such as polished bedrock surfaces, high valley flanks, moraine ridges, and outwash terraces. Moreover, large-scale features of this dynamic landscape include overdeepened valleys and basins that are hidden below the present-day surface in the Alpine valleys and the Alpine foreland (Preusser et al., 2010; Gegg and Preusser, 2023). These overdeepened structures mainly represent deep and elongated troughs eroded by glaciers into the bedrock below

the fluvial base level (Cook and Swift, 2012). The formation process of overdeepening is under debate but presumably is a combination of ice-contact processes (i.e., abrasion and plucking) and pressurized subglacial (melt)water erosion (Huuse and Lykke-Andersen, 2000; Alley et al., 2019). Substantial overdeepening is not limited to topographically confined, inner-Alpine valleys with steep gradients but is also found in the lower-relief Alpine foreland (Preusser et al., 2010; Ellwanger et al., 2011; Ellwanger, 2015). An increased availability of basal water is believed to have enhanced the subglacial erosional potential far into the Alpine foreland, thus becoming a driving force for erosion (Alley et al., 1997; Dürst Stucki et al., 2010; Dürst Stucki and Schlunegger, 2013; Gegg et al., 2021).

Foreland overdeepenings offer large accommodation space upon deglaciation, capable of hosting multiple stacked and nested glacial sequences within subglacial to proglacial sediment successions, as well as post-glacial deposits (Schlüchter, 1989; Preusser et al., 2005; Anselmetti et al., 2010; Dehnert et al., 2012; Buechi et al., 2018). These formations serve as valuable archives that provide insight into the timing and extent, as well as the subglacial conditions and processes, of past glacier advances in the northern Alpine foreland (Preusser et al., 2010; Ellwanger et al., 2011; Gegg and Preusser, 2023). To unravel the complex glacial dynamics that produced overdeepened landforms and their sedimentary fillings, a combination of coring and geophysical analysis has proven indispensable (e.g., Dehnert et al., 2012; Pomper et al., 2017; Buechi et al., 2018; Gegg et al., 2021). Recent studies have also benefited significantly from advances in dating techniques, such as optically stimulated luminescence (OSL) dating, revolutionizing our ability to precisely determine the timing of glacial advances (e.g., Preusser et al., 2005; Dehnert et al., 2012; Fiebig et al., 2014; Buechi et al., 2018; Schwenk et al., 2022).

Unfortunately, such scientific investigations of sedimentary successions are still scarce, while records of commercial drillings, usually with cuttings only, often lack the necessary detail for comprehensive sedimentological interpretation and geochronological constrains. To address this gap, the pan-Alpine project Drilling Overdeepened Alpine Valleys (DOVE) was initiated, co-funded by the International Continental Scientific Drilling Program (ICDP). DOVE aims to conduct detailed investigations at several complementary sites along the northern (and potentially southern) Alpine foreland (Anselmetti et al., 2022). The primary objective of DOVE is to determine the timing and extent of past Alpine glaciations and to contribute to broader discussions on climate teleconnections and synchronization of glaciations across the Northern Hemisphere. This study aims to contribute data to evaluate patterns in glacial–interglacial paleoclimates and landscape evolution from a key overdeepening of the Alpine foreland: the Tannwald Basin. This basin stands out in several distinct aspects, leading to its identification as a high-potential location for the DOVE project (Anselmetti et al., 2022). Situated in the region that formerly occupied the Rhine Glacier piedmont lobe, it has been repeatedly covered by ice; however, this was without experiencing the direct impact of the Last Glacial Maximum (LGM) (Ellwanger et al., 1995, 2011; Ellwanger, 2015).

2 Geological setting

2.1 Lake Constance amphitheater

The Rhine piedmont–glacial landscape, which stretches from the northern Alpine front to the Swabian Jura, bears the distinct imprint of Quaternary erosion and deposition processes. These dynamic geological forces have sculpted the terrain into an amphitheater-like topography within the Alpine foreland Molasse Basin (Ellwanger et al., 1995, 2011; Lämmermann-Barthel et al., 2003), with Lake Constance at the heart of it. While different Quaternary stratigraphic systems are in use in the countries that border Lake Constance (Doppler et al., 2011; Preusser et al., 2011), a stratigraphic framework for the Lake Constance amphitheater has been introduced (Fiebig, 1995; Ellwanger et al., 1995, 2011; Geyer et al., 2011). This approach comprises four regional unconformity-bounded units that represent the three distinct generations of basin formation: the Steinental Fm., Dietmanns Fm., Illmensee Fm., and Hasenweiler Fm. The formation boundaries of the youngest three correlate with pleniglacial conditions during the Hosskirch, Riss (both Middle Pleistocene), and Würm (Late Pleistocene) glaciations, respectively (Ellwanger et al., 2011; Fig. 1). These lithostratigraphic investigations, in addition to the morphostratigraphic concept, have furthermore increased knowledge of changes in the erosion pattern and the identification of the reorientation of the branch glacial basins over time. While alignment of branch basins was originally northward towards the Danube, the direction later shifted into a westward direction towards the "Hochrhein" Rhine. This change in glacial direction also modified the fluvial drainage network orientation, i.e., the Alpine Rhine was connected to the lower parts of the Rhine drainage system (Ellwanger et al., 1995, 2011).

2.2 Previous drillings and geophysical surveys in the Tannwald Basin

Within the Lake Constance amphitheater, some overdeepened basins have been influenced by multiple glaciations (Ellwanger et al., 2011). One notable example of an overdeepened structure that has witnessed multiple glaciations is the Tannwald Basin, a distal overdeepened branch basin located ca. 45 km north of Lake Constance. It became of significant importance when pollen indicative of the Holsteinian Interglacial, the equivalent of Marine Isotope Stage (MIS) 11, were identified in a fine-grained lacustrine sediment succession of a research drilling in 1993/1994 ("Schneidermartin" drilling; Ellwanger et al., 1995, 2011;

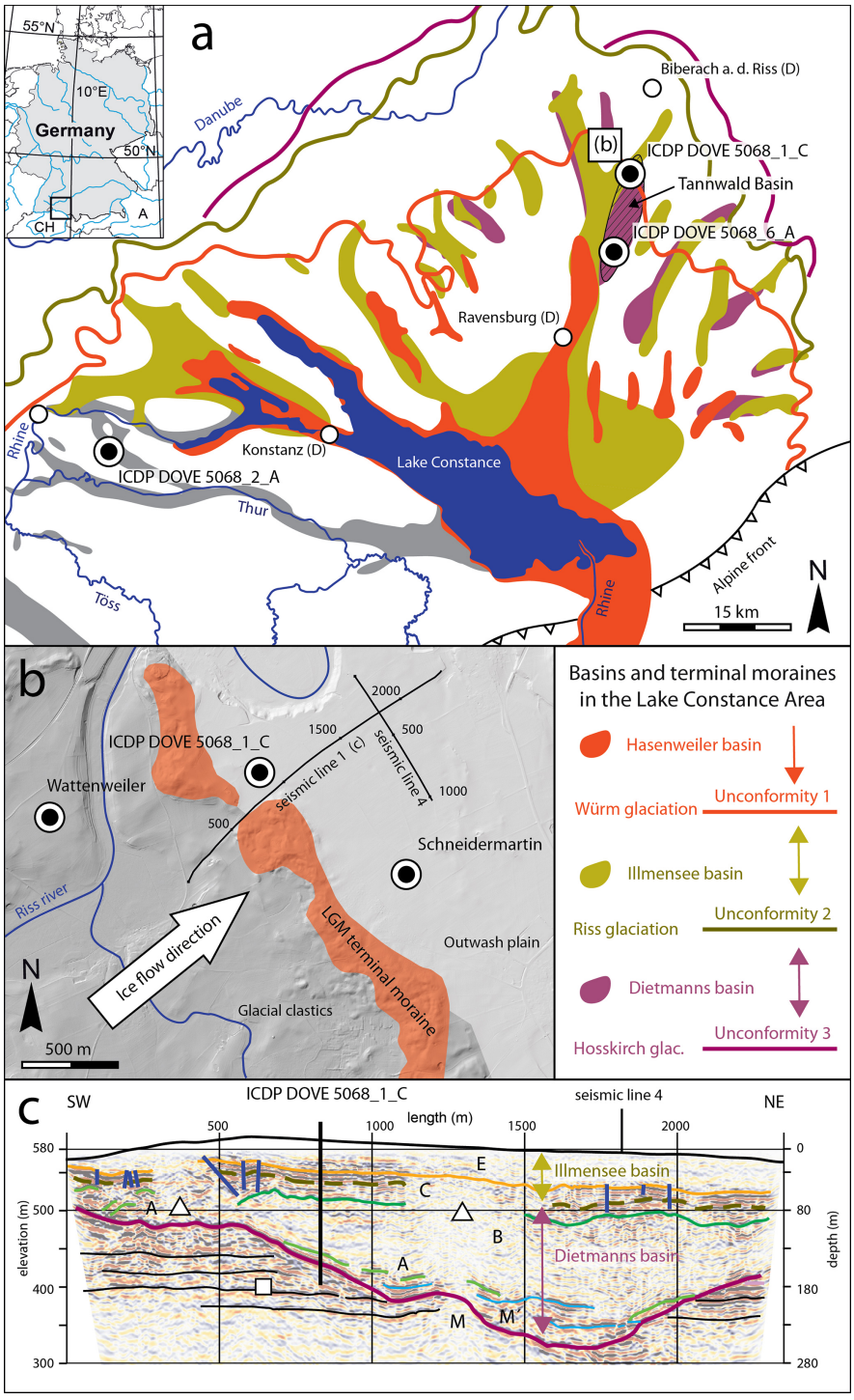

Figure 1. **(a)** Map illustrating the Quaternary overdeepened structures within the German (differentiated) and Swiss (undifferentiated) Lake Constance area of the Rhine glacial landscape in the northern Alpine foreland. The location of the Tannwald Basin is indicated by a black area with hatching. Shown are the maximum ice advances corresponding to the respective glaciations (regional unconformities 1–3); modified after Graf (2009) and Ellwanger et al. (2011). **(b)** Locations of seismic survey and new drill site (ICDP DOVE 5068_1_C) with respect to the outermost terminal moraine of the last glaciation (equivalent to unconformity 2, modified after Burschil et al., 2018). **(c)** Seismic section displaying interpreted geological structures based on the stratigraphy of the Schneidermartin core. Seismic facies abbreviations: M (purple lines) represents molasse, M′ (blue lines) represents slabs of allochthonous molasse, A (light green lines) represents waterlain till, B (dark green lines) represents fine-grained deposits, C (lines of same color as unconformity 2) represents till and sand units, E (orange lines) represents fluvial sand and gravel. Blue vertical line: faults with offsets > 2 m. White square: foresets. White triangle: seismic transparent regions. Modified after Burschil et al. (2018).

Hahne et al., 2012). The Schneidermartin drilling is located just outside the terminal moraine ridge of the LGM (Fig. 1b) and reached the Molasse bedrock at the base of the basin, at 209 m depth. Similar pollen assemblages were identified in the Wattenweiler drilling, situated ∼3500 m northwest of the Schneidermartin drilling within the LGM terminal moraine (Hahne et al., 2012; Ellwanger, 2015). The pollen findings were used to assign the Tannwald Basin to the pre-Holsteinian (pre-MIS 11) advance of the Hosskirch glaciation (Ellwanger et al., 2011). A detailed revision of the sedimentary succession of the Schneidermartin core projected the erosional unconformity 2 of the Riss glaciation (MIS 6) to a depth of 29 m (Ellwanger, 2015; Burschil et al., 2018). Consequently, the Tannwald Basin was interpreted to contain sedimentary deposits representing two generations of basins (Dietmanns Formation, Illmensee Formation) and two glacial cycles (Riss, Hosskirch).

The infill of the Tannwald Basin at the Schneidermartin drilling (Ellwanger et al., 2011) comprises thin layers of sheared fine-grained sediments above the undisturbed Molasse bedrock. These are overlain by a 13 m thick glacially sheared block of Molasse, containing several shear horizons. Based on seismic data, this block has been interpreted as an allochthonous bedrock slab (Burschil et al., 2018). It is overlain by gravel layers with Molasse components, followed by diamictic fines, which were interpreted to represent ice-proximal sediments of the Hosskirch glacial period. Above, a succession of delta bottomsets hosts the previously mentioned pollen assemblages assigned to the Holstein Interglacial. Upcore, these sediments transition into foresets that are capped by a till layer, exhibiting stratification and grading, evolving into a matrix-supported diamict and fines. This layer is separated from topmost coarse gravels, which represent meltwater deposits of the Würm glaciation, by an unconformity.

Five P-wave seismic reflection profiles were acquired in the northeastern section of the Tannwald Basin during 2014/2015 (Burschil et al., 2018). Based on the seismic data and the Schneidermartin drill core description, Burschil et al. (2018) identified six seismic facies and traced them across the five profiles (Fig. 1c). Furthermore, the seismic campaigns revealed a 50 m deep and several 100 m wide depression inside the basin, marking its deepest parts. Several faults with offsets >2 m were identified within the upper 100 m of the basin fill (Burschil et al., 2018). A complementary acquired 3D multicomponent S-wave dataset allowed us to visualize more reflections and lead us to the identification of glacial tectonics, including additional faults and shallow glaciotectonic cuspate–lobate folds (Buness et al., 2020, 2022).

3 Methods

3.1 Drilling operations

Drill site ICDP DOVE 5068_1, located on the western flank of the overdeepened Tannwald Basin, was the first of the DOVE sites to be drilled in April 2021 (Fig. 1c; Anselmetti et al., 2022). To facilitate correlation, it was strategically positioned near the seismic profiles and the Schneidermartin drill site (Fig. 1b). Besides the core drilling ICDP 5068_1_C, two flush drillings (ICDP 5068_1_A and -B), arranged in a triangle with side lengths of 28 m, were drilled to allow for a later cross-hole seismic campaign. The primary challenges encountered during the drilling of the Tannwald Basin were caused by large variations in grain size and the unconsolidated nature of the sediments. To address these challenges, the drilling team adopted a combined approach, utilizing percussion coring techniques down to a depth of 83 m, below which a wireline rotational core system was used that reached the final depth of 166.25 m. For a comprehensive overview of the drilling and logging operations, core-quality assessment, and technical parameters (such as borehole geometry and casing deployment), see the DOVE operational report (DOVE-Phase 1 Scientific Team, 2023a).

The core drilling ICDP DOVE 5068_1_C successfully retrieved 200 individual core sections, each stored within opaque PVC liners with an inner diameter of 104 mm. The overall recovery rate was 95 %, some core loss occurred primarily in unconsolidated coarse gravels and cobbles above 39 m depth. Additionally, the unconsolidated nature of the sediments led to the mobilization and partial loss of sandy and fine sediments, for example at depths between 70 and 115 m. Both at the drill site and university storage facilities, the cores were refrigerated at 3–5 °C.

3.2 Core logging and sampling

The core workflow defined in the DOVE project follows mostly the guidelines developed during the Quaternary drilling campaign of the National Cooperative for the Disposal of Radioactive Waste of Switzerland (e.g., Schuster et al., 2020), which has been successfully applied in numerous drilling campaigns within the Swiss Alpine foreland (e.g., Gegg et al., 2021; Schaller et al., 2023). We conducted non-destructive, whole-core scanning to measure wet bulk density and magnetic susceptibility, using a multi-sensor core logger (MSCL; Geotek Ltd.) at 5 mm resolution. Any disturbed segments encountered during drilling or described in the lithological analysis were later manually excluded. A baseline correction was applied to the magnetic susceptibility data. Subsequently, the cores were split into archive and working halves (A-half and W-half) under subdued orange light to facilitate luminescence dating at a later stage.

The initial core description (ICD) was carried out on the A-half with a primary focus on specific sedimentological ob-

servations, including grain size, character of contacts (e.g., erosional or deformed), clast characteristics (e.g., shape and roundness), clast-surface features (e.g., striations and calcite precipitations), and sedimentary structures (e.g., cross-bedding, lamination, and grading). High-resolution line-scan images were generated with the Geotek scanner to support the ICD. Additionally, we conducted minimally invasive measurements using a vane-shear tester to systematically estimate the undrained shear strength, where the sediment was suitable (i.e., dominantly sand or finer). We selected specific cores, primarily those suspected to contain ice-contact sediments, for X-ray computed tomography (CT) scanning at the Institute of Forensic Medicine, University of Bern. Subsequently, observations from geophysical logs, ICD, and CT scans were integrated to define lithotypes, following Eyles et al. (1983) and Schaller et al. (2023). On the basis of the sedimentary characteristics and context, the lithotypes were grouped into seven lithofacies assemblages (LFAs). These LFAs then serve as building blocks to establish three lithostratigraphic units, which in turn constitute the foundation of the geological interpretation.

The W-half was used for destructive sampling under subdued orange light, while all cores were otherwise stored in lightproof tubular film. Geochemical samples were taken immediately upon opening the cores at a 1 m resolution. These samples were also used to determine water content. Subsequently, the fine fraction (< 63 µm) of the geochemical samples was analyzed for their carbon content, including total organic carbon (TOC) and total inorganic carbon (TIC), using a Thermo Scientific Flash 2000 Smart (Thermo Fisher, Waltham, MA, USA). The concentrations of carbonates and organic matter (weight percent) were calculated by multiplying TIC and TOC values by the stoichiometric factors of 8.3 and 1.8, respectively (Meyers and Teranes, 2001). Potential downcore variations in carbonate phases, such as the dolomite/calcite ratio, were, however, not accounted for. For further information on the curated samples, analysis, and data, see the operational dataset (DOVE-Phase 1 Scientific Team, 2023b) and explanatory remarks (DOVE-Phase 1 Scientific Team, 2023c).

4 Identification and interpretation of lithotypes and lithofacies associations

Seventeen lithotypes (facies codes in italic) were identified in the ICDP DOVE 5068_1_C core (Fig. 2), 11 of these follow those introduced by Schaller et al. (2023), while 6 lithotypes are unique to the Tannwald drill core. These lithotypes are presented as core photos (Figs. 3 and 4) and detailed descriptions in the Appendix (Table A1). The broad range of lithofacies encountered in the ICDP DOVE 5068_1_C core was reduced by grouping commonly associated lithofacies into seven lithofacies associations (LFAs; Fig. 2 and Table 1).

The bottom of the ICDP DOVE 5068_1_C core consists of moderately consolidated, partly friable sand- and siltstones, and marls, all representing Molasse bedrock (*B*, Fig. 3a). The Molasse was identified as the Upper Marine Molasse (tOM according to the nomenclature of Ellwanger, 2015; Bachmann et al., 1987) as opposed to the interpretation of the seismic data (Upper Freshwater Molasse; Burschil et al., 2018). A sharp, planar bedrock contact at 155.90 m depth marks the erosional base of the Tannwald overdeepening in the core.

LFA1 is located directly above the bedrock and predominantly comprises both unconsolidated (Fig. 3b) and consolidated (Fig. 3c) Molasse bedrock rafts (*Mgt*). Glauconite grains identify the bluish sand of the unconsolidated Molasse rafts as Upper Marine Molasse (Fischer, 1987). The consolidated Molasse rafts show in situ crushing and brecciation. The Molasse bedrock rafts are intercalated and locally sheared into stratified diamicts (*Dms*). *Dms* of LFA1 contains glacially striated clasts of Alpine lithologies and substantial amounts of friable bedrock fragments. LFA1 is defined by low density ($2\ \mathrm{g\ cm^{-3}}$) and shear-strength values below 50 kPa of the unconsolidated Molasse bedrock rafts. The deformation structures and weak mechanical properties are interpreted as evidence of the shearing of subglacial till and bedrock rafts (Benn and Evans, 1996; Hiemstra and van der Meer, 1997; Buechi et al., 2017). Carbonate content reaches below 20 wt %, which further reflects the incorporation of local Molasse sediments into LFA1. Therefore, LFA1 is classified as a Type B glaciotectonite (Benn and Evans, 1996; Evans et al., 2006).

LFA2 comprises brownish-colored, matrix-supported, massive, and stratified diamicts (*Dmm, Dms*) associated with well-sorted, fining-upward sediments that contain frequent dropstones (*Flr(d), Fl(d), Sl*). The stratified fines located between the basal diamicts do not exhibit macroscopic deformation features at the core scale. The number of dropstones generally increases near the diamicts, indicating the presence of floating ice (Bennett et al., 1996; Eyles et al., 1983). Both dropstones and diamicts frequently contain clasts with glacial striations, providing further evidence for the proximity of the glacier. Even though the organic matter content is very low (mostly < 0.5 wt %) throughout the core, it abruptly increases from 0.1 to 0.3 wt % at the emplacement of the matrix-supported diamicts (*Dmm*; Fig. 3d) of LFA2. Furthermore, *Dmm* exhibits both high values of density ($2.4\ \mathrm{g\ cm^{-3}}$) and shear strength (200–270 kPa), with low water content (10 %–13 %). A similar shift of shear-strength values measured in drill cores from a glacial overdeepening has previously been interpreted as the result of temporary ice loading (Anselmetti et al., 2010; Dehnert et al., 2012). Alongside frequent glacial striations, this observation likely indicates subglacial lodgement processes. Consequently, *Dmm* is interpreted as subglacial till (Evans et al., 2006), suggesting that LFA2 was emplaced subglacially or submarginally with intermittent glacier–bed coupling. The association with stratified fines (*Flr(d), Fl(d)*) and diamicts (*Dms*) further sug-

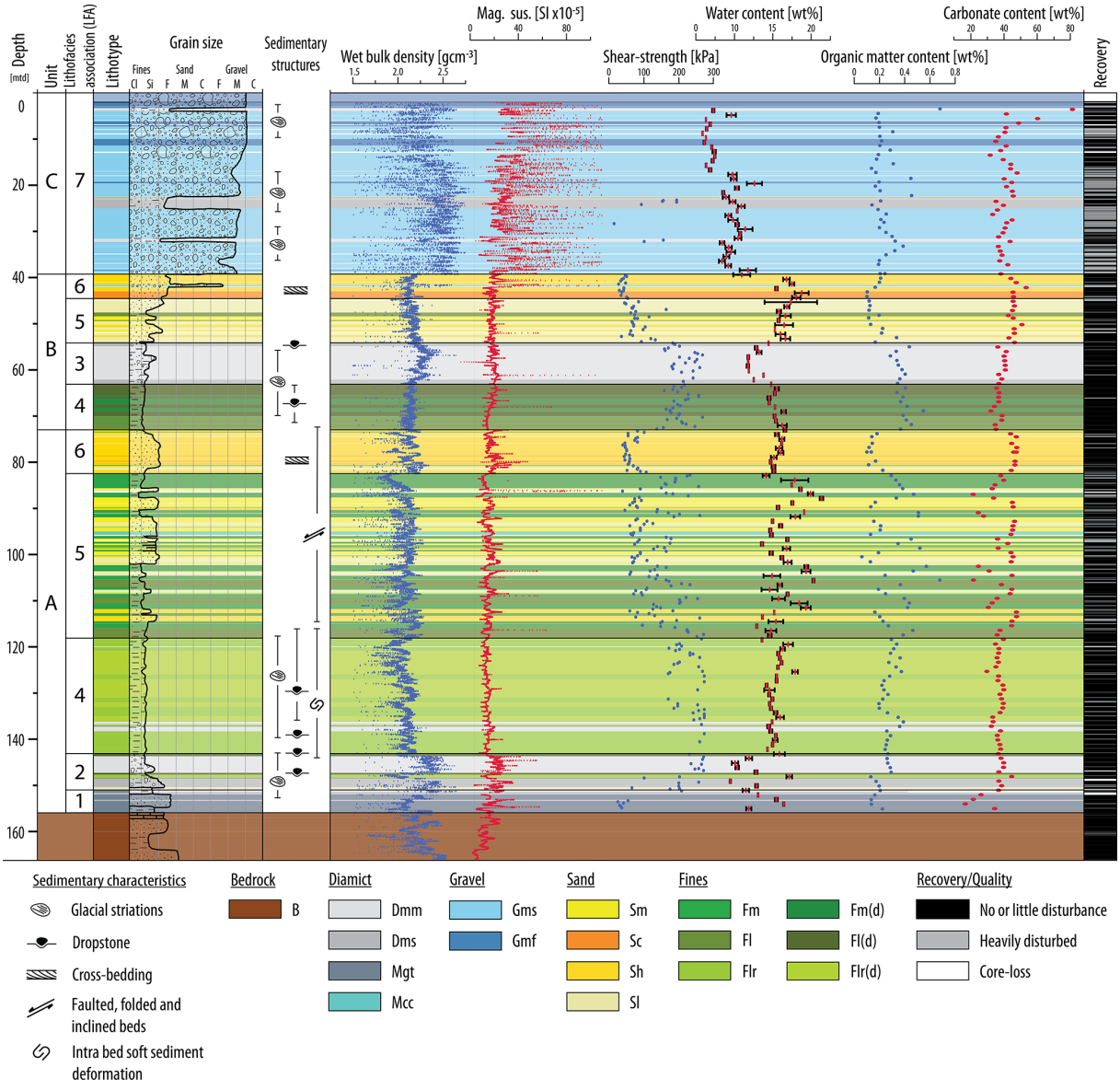

Figure 2. Summary profile of the ICDP DOVE 5068_1_C core with sedimentary characteristics and acquired petrophysical data.

gest deposition during ice–bed decoupling in confined subglacial cavities or infilling of accommodation space created under a floating glacier tongue (Ravier et al., 2014; Buechi et al., 2017).

LFA3 consists of fine-grained *Dmm* deposits of dark grey color with frequently occurring glacially striated clasts (Figs. 2, 3e). The *Dmm* deposits show increasing density upcore (peak at 56 m; 2.4 g cm^{-3}), which reflects a gradual increase in clast size upcore (Fig. 2). Upcore-increasing shear strength (peak at 57 m; 270 kPa) additionally indicates increasing compaction. Water content reaches its lowest values of 14 % at 58 m. Thus, LFA3 is interpreted to be similar to LFA2 as a mud-dominated subglacial till (Evans et al., 2006). The fine-grained character and dark grey color are attributed to the predominant incorporation of underlying glaciolacustrine deposits.

LFA4 consists of fine-grained deposits with gradual laminations and beds, often containing dropstones (*Flr, Flr(d), Fl, Fl(d)*; Fig. 4d, g, c, f) and rarely interbedded with soft, dark-colored, and fine-grained diamicts (*Dmm*, Fig. 3e). Frequent glacial striations on both dropstones and diamicts suggest the proximity of a glacier. The diamicts show low density values (2.2 g cm^{-3}) and relatively low shear strength (compared to the overlying fines) and are interpreted as subaqueous debris flows with a proglacial sediment source (Eyles et al., 1983; Mulder and Alexander, 2001). LFA4 is interpreted as deposits from an ice-contact proglacial lake. The fines of LFA4 at around 70 m depth of the ICDP DOVE

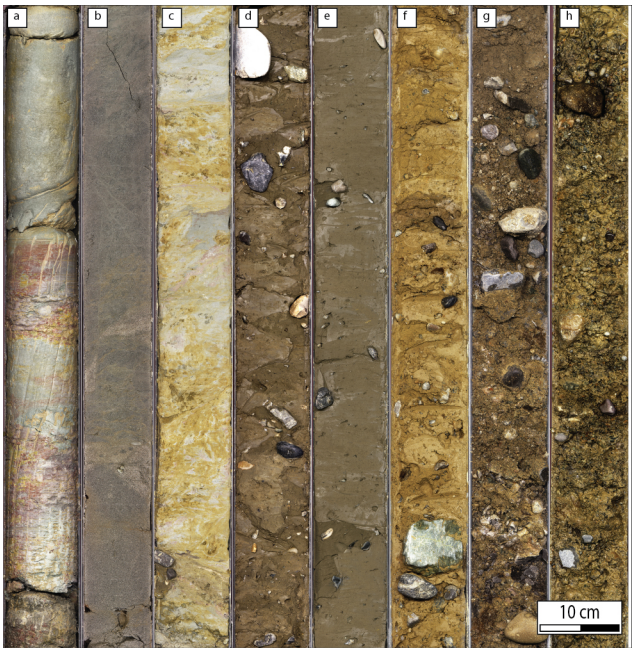

Figure 3. Line-scan images of cores (1 m sections), showing representative lithotypes. **(a)** *B*: interbedded mottled siltstone and sandstone of the Molasse bedrock (163–164 m). **(b)** *Mgt*: unconsolidated and deformed (faulted) medium sand of the Molasse bedrock (153–154 m). **(c)** *Mgt*: consolidated and deformed Molasse siltstones and sandstones associated with small amounts of diamict (mélange type) (152–153 m). **(d)** *Dmm*: highly consolidated, brownish-colored diamict with both Alpine and Molasse clasts (144–145 m). **(e)** *Dmm*: soft, fine-grained, dark-colored diamict (57–58 m). **(f)** *Dms*: soft, light-colored diamict (23–24 m). **(g)** *Gms*: moderately sorted gravel with sandy matrix (10–11 m). **(h)** Gmf: poorly sorted gravel with silty and sandy matrix, likely partly washed out during coring (10–11 m).

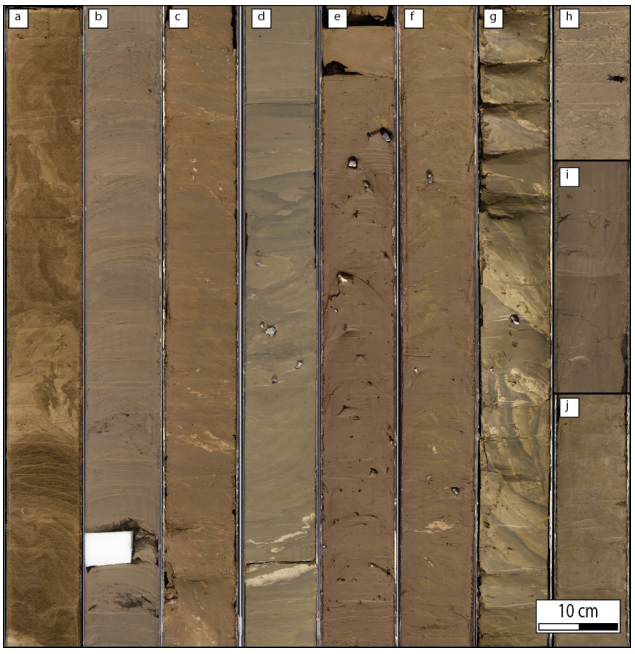

Figure 4. Line-scan images of cores (1 and 0.5 m sections) showcasing representative lithotypes. **(a)** *Sh/Sc*: partly deformed (homogenized), brownish-colored, (cross-)bedded fine to medium sand (78–79 m). **(b)** *Sh/Sl*: dark-colored, fine sand interbedded with dark silt and clay laminae (53–54 m). **(c)** *Fl*: mottled laminations in clay and silt (lighter greenish and darker grey shades) with bright sand laminae and sand lenses (106–107 m). **(d)** *Flr*: deformed silt and clay rhythmites of varying thicknesses (126–127 m). **(e)** *Fm(d)*: massive fines with dropstones (66–67 m). **(f)** *Fl(d)*: mottled lamination in clay and silt with sandy laminae, soft sediment deformation and dropstones (64–65 m). **(g)** *Flr(d)*: highly consolidated rhythmites with dropstones and strong soft sediment deformation (118–119 m). **(h)** *Mcc*: fine to medium sand with horizontally aligned silt and clay lenses (107–107.5 m). **(i)** *Sl*: oversteepened beds of laminated fine sand (94–94.5 m). **(j)** *Fm*: massive fines (84.5–85 m).

5068_1_C core show a slight upcore-increasing trend in density and shear strength (if a trend is visible at all), while water content decreases upcore. Increasing amounts of dropstones upcore illustrate the shift from more distal, well-sorted clay and silt facies to a proximal, dropstone-dominated facies with frequent glacial striations. This typical upward succession can be interpreted, similarly to LFA2 and LFA3, as evidence of glacial approaching and overriding. However, the trend in density and shear strength might alternatively result from an upcore decrease in clay content. Multiple meter-thick beds of fine-grained lake sediments (*Flr(d)*) at a depth of 119–115 m show similar petrophysical characteristics and are moreover above-average consolidated (Fig. 4g). This also suggests compaction from ice contact, indicating a glacial advance (Anselmetti et al., 2010; O'Regan, 2010; Dehnert et al., 2012). The fines in the lower part of the core locally exhibit soft-sediment deformation along several horizons, ranging from centimeter-thick slumps to meter-thick deformed sections (Fig. 4d). Deformation mechanisms include both faulting and folding and, within water-saturated fines on a depositional slope in subglacial to proglacial beds, likely indicate gravitational slumping (Visser et al., 1984).

LFA5 is characterized by intercalated meter-thick successions of stratified and massive fine-grained deposits (*Fm, Fl*; LFA5.1) and greyish-colored, partly laminated sands (*Sm, Sl*; LFA5.2). The intercalation results in varying density values and a significant scatter in shear-strength values in beds of cohesive fines and uncohesive sands. Carbonate content varies between 20 wt % and 40 wt %, indicating varying sediment sources (Alpine and Molasse origin). Post-sedimentary deformation occurs throughout LFA5 is in the form of folding, faulting, and inclined bedding. *Fm* and *Fl* are interpreted as the product of turbidity currents and suspension settling in an ice-proximal lake (Eyles et al., 1993; Smith and Ashley, 1985), while the sand-dominated facies is attributed to density flows (Mulder and Alexander, 2001) and subaqueous channel fills in a higher energy setting. The repeated shifts between LFA5.1 and LFA5.2 are attributed to

transitions to a more proximal or laterally shifted deltaic setting (Dehnert et al., 2012). The dark grey laminations in the sand beds (Fig. 4b) suggest that this process occurs not only on the meter scale but also on the centimeter scale. The post-sedimentary deformation features along multiple failure surfaces, which are likely the result of reduced slope stability during interglacial periods. A similar phenomenon of slope instability that resulted from geomorphological changes during rapid deglaciation has been documented by Fernandes et al. (2020) in the Central Pyrenees. Furthermore, LFA5 contains horizontally aligned, decimeter-thick beds of mud-clasts, which are interpreted as reworked fine lacustrine sediments eroded by subaquatic mass movements (Li et al., 2017). These beds were also identified as mud-clast conglomerates (*Mcc*; Fig. 4h) in the ICDP_5068_2 core (Schaller et al., 2023).

LFA6 is characterized by well-sorted, massive, and stratified sands (*Sh, Sc*) of brownish color that are weakly consolidated and rarely interbedded with moderately sorted gravel (*Gms*; Fig. 3e). LFA6 is strongly deformed in the lower part of the core, mainly through steep to near-vertical bedding (Fig. 2). These sands and gravels are interpreted as glaciodeltaic deposits, formed by underflows from the retreating glacier front during deglaciation (Buechi et al., 2018). This interpretation is supported by a change in color (Fig. 4a), indicating a shift in the primary sediment source of basinal fines.

LFA7 consists of moderately sorted gravels with sand-dominated matrix (*Gms*) and poorly sorted gravels with predominantly fine-grained matrix (*Gmf*; both LFA7.1) with intercalated soft matrix-supported light-colored diamicts (*Dmm, Dms*; LFA7.2). Both the gravels and the diamicts frequently show glacially striated clasts, which indicate a glacier-proximal depositional environment. Thus, LFA7 is interpreted as proglacial fluvial and glaciofluvial sediments, representing alternating meltwater outwash and subaerial debris flows, possibly sourced in ice-marginal and supraglacial sediments (e.g., Lawson, 1982; Buechi et al., 2018). *Dmm* and *Dms* exhibit comparatively low shear-strength values that support interpretation of a non-subglacial origin (< 200 kPa). Thus, they partly exhibit characteristics of subglacial till (massive nature, glacial striations), but they lack consolidation (low density and shear strength). Thus, diamicts of LFA7 are interpreted as short-distance redeposition by slumping of diamicts, originally deposited at the LGM glacier front on the inclined outwash plain (Fig. 1b; Ellwanger et al., 2011). *Gmf* likely represents sedimentation in a more chaotic setting, possibly during a more proximal glacier position or during floods (Eyles et al., 1983; Siegenthaler and Huggenberger, 1993). The upcore-increasing occurrence of *Gmf* correlates with an increase in carbonate content and occurrence of cobble-sized clasts, reflected in an increase in density (Fig. 2), which might indicate an overall shift to a more ice-marginal position in a fluvial and glaciofluvial proglacial outwash plain.

5 Discussion

The lithostratigraphic and petrophysical observations of the sedimentary infill in the Tannwald Basin are integrated with existing seismic data (Burschil et al., 2018; Buness et al., 2020, 2022), morphostratigraphic data, and previously published drill-core data (Ellwanger et al., 2011; Hahne et al., 2012). To facilitate this integration, the Quaternary sedimentary infill was categorized into three lithostratigraphic units: A, B, and C (Fig. 2). These units represent distinct episodes of basin infill separated by stratigraphic breaks (Figs. 5 and 6).

The facies evolution in Unit A is interpreted as basin erosion and subglacial traction processes (LFA1 and LFA2; Fig. 5a), followed by ice-proximal sedimentation in a proglacial lake (LFA4; Fig. 5b), and eventually a glacier retreat leading to the formation of a stacked delta succession (LFA5 and LFA6; Fig. 5c). The bedrock rafts of LFA1 can be correlated with mobilization and transport of much larger (> 10 m) rafts reported from the Schneidermartin core (Ellwanger et al., 2011; Hahne et al., 2012) and seismic facies M′ of the seismic survey at deeper positions of the Tannwald Basin (Burschil et al., 2018; Fig. 6). The overlying LFA2 was probably still emplaced in a subglacial to submarginal setting, as indicated by the intimate association of subglacial traction till with sorted fines and stratified diamicts. The interbedding is likely to represent first a coupled and then a decoupled ice–bed interface, as a result of an oscillation of the ice-margin position, intermittent floating of the glacier tongue, or opening and closing of more confined subglacial cavities (Fig. 5a). LFA2 correlates with seismic facies A on the western slopes of the Tannwald Basin (Burschil et al., 2018; Fig. 6). The overlying LFA4 represents typical fine-grained, dropstone-bearing basin fill observed in ice-contact proglacial lake, representing turbidity flows on a subaqueous fan (Fig. 5b). They can be correlated with finer basin-floor bottomsets of the Schneidermartin drill core 1 km SW further away and seismic facies B (Ellwanger et al., 2011; Burschil et al., 2018; Fig. 6). The organic matter content does not indicate interglacial sediments, suggesting the filling of the overdeepening under still periglacial conditions, which is a common phenomenon (Gegg and Preusser, 2023). Individual beds of above-average consolidated fines at the top of LFA4 might result from compaction by ice contact, indicating glacial advance (Anselmetti et al., 2010; O'Regan, 2010; Dehnert et al., 2012). However, the role the glacier played within this lake remains an open question, especially because of the lack of coarse-grained deposits that are expected at the front of a moving glacier. One possible explanation might be the reported inability of such re-advances to carve basins into fine-grained, soft lake sediments with low permeability (e.g., Menzies, 1989). The onset of delta propagation might be associated with continuing and larger-scale gravitational slumping on the depositional slopes of the basin, leading to faulted and folded sediment beds. This correlates with the

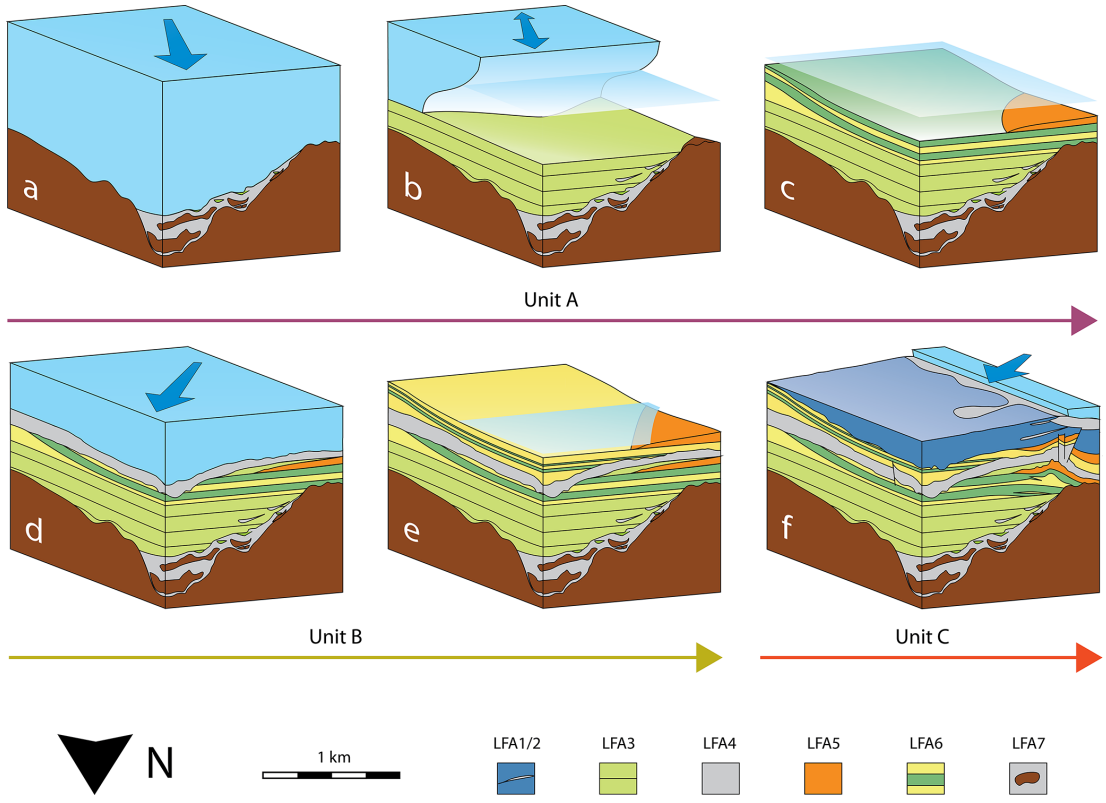

Figure 5. Schematic block diagrams to illustrate the geological evolution of the Tannwald Basin. Glacier ice is illustrated in light blue, water level in transparent light blue, and (oscillating) ice-flow direction with dark blue (bi)directional arrows. **(a)** Advancing glacier from S (Hosskirch glaciation), basin erosion and transport of bedrock rafts and subglacial diamict, filling of subglacial cavities at decoupled ice–bed interfaces. **(b)** Ice-contact sedimentation in proglacial lake with mass movements on basin slopes. **(c)** Glacier retreat and stacked delta formation. **(d)** Glacier re-advance from SW (Riss glaciation) and erosion of second-order inlaid basin. **(e)** Glacier retreat and stacked delta formation. **(f)** Glacier advance from SW (Würm advance, LGM), emplacement of LGM terminal moraine with mass movements on outwash plain, glaciotectonic deformation of sedimentary strata of Unit A.

transition from fine-grained bottomsets to foresets inferred from the Schneidermartin core at the top of seismic facies B (Ellwanger et al., 2011; Burschil et al., 2018; Fig. 6). The facies evolution from LFA5 to LFA6 with fluvial channel fills of different color indicates the transition to a more proximal sediment source, for example, by development of alluvial fans by more local, secondary stream-networks after glacial retreat (Fig. 5c). Finally, Unit A is identified as the Dietmanns Formation (Ellwanger et al., 2011; Hahne et al., 2012).

Facies evolution of Unit B indicates glacier re-advance, likely coupled with secondary shallow basin erosion (LFA4 and LFA3; Fig. 5d), subsequent glacier retreat, and, in analogy to Unit A, delta formation (LFA5 and LFA6; Fig. 5e). In contrast to the Schneidermartin core, where coarsening-upward foresets announce glacier advance (Ellwanger et al., 2011), the ICDP DOVE 5068_1_C core shows the transition back to fine-grained lacustrine sediments. The characteristics (dropstone occurrences, density) of LFA4 indicate gradual glacier advance, infilled into a newly eroded, possibly rather shallow, basin, stacked on top of the main valley fill (Fig. 5d). This is supported by the fact that overlying LFA3 correlates with unconformity 2 (Fig. 1c) and can be followed in the seismic profiles of Burschil et al. (2018) from the Schneidermartin core at ∼ 30 m depth (Ellwanger et al., 2011) to the ICDP DOVE 5068_1_C core at ∼ 60 m depth (Fig. 6). Hence, Unit B is identified as the Illmensee Formation (Ellwanger et al., 2011; Hahne et al., 2012).

Unit C indicates the development of a fluvial and glaciofluvial proglacial outwash plain with mass movements from the close glacier margin (LFA7; Fig. 5f). LFA7 morphologically correlates with the outwash plain associated with the LGM terminal moraine ∼ 100 m to the southwest of the ICDP DOVE 5068_1_C drilling (Figs. 1b, c and 6). The basal contact of LFA7 can be followed in the seismic profiles of Burschil et al. (2018) to the Schneidermartin core (Ellwanger et al., 2011), where it correlates to the topmost 22 m of fluvial coarse gravels with diamicts. The decreased thickness at the Schneidermartin drilling might be due to the greater distance from the LGM terminal moraine. The LGM glacier,

https://doi.org/10.5194/sd-33-191-2024

Table 1. Summary table of lithofacies associations (LFAs).

Lithofacies association		Facies codes	Short description	Base contact	Interpretation
LFA1 Diamicts with bedrock fragments/rafts		*Mgt, Dms*	Tectonically sheared bedrock fragments and matrix-supported stratified diamict of brownish color ranging to Molasse color	Sharp	Glaciotectonized bedrock, proto-till
LFA2 Diamicts with sorted interbeds		*Dmm, Dms, Flr(d), Fl(d), Sl*	Brownish-colored and highly consolidated diamict with glacial striations intercalated with graded sand, silt and clay with lamination and frequent dropstone occurrences	Gradual	Subglacial till with subglacial cavity fills
LFA3 Matrix-rich diamicts		*Dmm*	Dark-colored fine-grained consolidated massive diamict	Unclear	Subglacial till
LFA4 Laminated silt and clay with diamictic interbeds		*Flr, -(d),Fl, -(d), Fm, -(d), Dmm*	Well-sorted dark-colored silt and clay with laminations and frequent dropstones, rarely associated with dark-colored fine-grained soft massive diamict	Gradual	Proglacial lake deposits with rare proglacial subaqueous debris flows
LFA5 Distal fan deposits	LFA5.1	*Fm, Fl*	Well-sorted massive to crudely laminated fines	Sharp or gradual	Distal fan deposits
	LFA5.2	*Sm, Sl*	Moderately sorted dark-colored sands with repeated laminae and beds of dark-colored silt and clay	Sharp or gradual	Distal to proximal fan deposits
LFA6 Proximal fan deposits		*Sh, Sc, Gms*	Well sorted brownish-colored cross-bedded and horizontally bedded sands with gravel interbed	Gradual	Proximal fan or subaqueous channels deposits
LFA7 Gravels with interbedded diamicts	LFA7.1	*Gms, Gmf*	Moderately to poorly sorted gravels	Sharp	Glaciofluvial outwash
	LFA7.2	*Dmm, Dms*	Light-colored fine- and coarse-grained soft diamicts	Sharp	Terrestrial debris flows

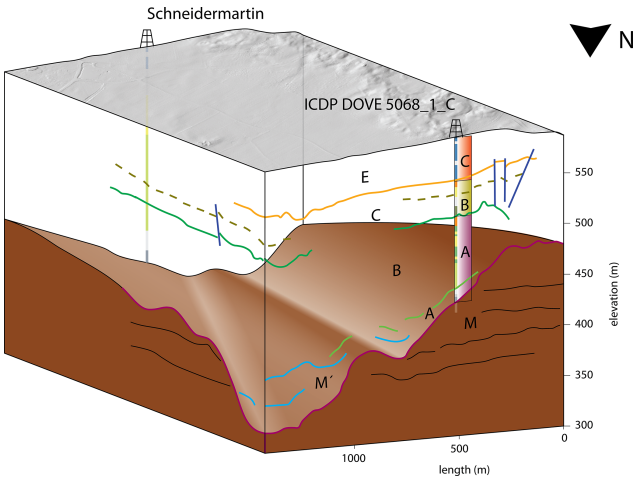

Figure 6. 3D block image showing simplified core profiles (of DOVE 5068_1_C (supplemented with the lithostratigraphic units of this study) and Schneidermartin (Ellwanger et al., 2011)) and their spatial relationship to seismic lines 1 (front) and 4 (left side) including the seismic facies (capital letters and colored lines; see Fig. 1c for legend; Burschil et al., 2018). Inferred bedrock morphology in brown, modern topography in grey.

which evidently created push-moraines in the Lake Constance area (Ellwanger et al., 2011), caused cuspate–lobate folding that was documented in 60 m depth in the vicinity of the ICDP DOVE 5068_1_C drilling (Buness et al., 2022). Seismic reflections of seismic line 1, however, seem to be displaced and inclined at an even greater depth of ~ 100 m (Fig. 1c). This effect can be correlated to sedimentary deformation in the form of faulting, folding, and oversteepening of sedimentary strata in LFA5 and LFA6 of Unit A (Figs. 2 and 6). Hence, glaciotectonic deformation caused by the Würm (LGM) glacial advance presents an alternative explanation to syn-sedimentary gravitational slumping. The resulting stresses might have further contributed to the above-average consolidation and severe deformation of fines at the interface of LFA4 and LFA5 of Unit A, as well as the mottled character of lamination of fines throughout Unit A.

6 Conclusions

Drilling the overdeepened Tannwald Basin revealed key geological and sedimentological features, including a basal 5.4 m thick glacial shear zone of deformed bedrock as well as recurrent ice-contact sediments. Frequent evidence of sediment deformation indicates the pivotal role of gravitational and glaciotectonic processes on the western slope of the basin. Detailed sedimentological investigations, combined with petrophysical data from the ICDP DOVE 5068_1_C core, led to the definition of seven lithofacies associations that were grouped into three lithostratigraphic units. Unit A represents an initial basin infill cycle following subglacial erosion and deformation, followed by the development of a delta. Unit B provides evidence for a glacier re-advance, once again followed by the development of a delta similar to Unit A. Unit C indicates the development of a glacier-proximal glaciofluvial outwash plain. Hence, the sedimentary sequence of the Tannwald Basin reflects a multi-phase stacked infill, indicative of at least three distinct glacial advances. However, without independent age control, the timing and relevance (glacial fluctuations or independent glaciations) of these advances remains uncertain.

The identification of potential ice-contact sediments (subglacial till) and indirect evidence of glacier overriding (sediment deformation and compaction) are crucial to interpret glacial sequences (not only within the Tannwald Basin). This task is particularly challenging in overdeepened basins, often accessed through drilling, which limits the scale and lateral continuity of observations and has rarely been carried out in detail (e.g., Buechi et al., 2017). In this context, 3D analysis, such as computer tomography (CT) scanning, will provide a powerful tool to identify and quantify sedimentological features and systematically characterize potential ice-contact sediments. To address the architecture of the sedimentary infill at the drill site, particularly in terms of shear-wave anisotropy and its sedimentological significance, a high-resolution cross-hole seismic survey has been conducted. Furthermore, luminescence and cosmogenic nuclide dating offer the potential of numerical age determination. The availability of such data will allow for an integration of the results into the broader context of the glacial evolution of the Lake Constance amphitheater.

Appendix A: Lithofacies description

Table A1. Summary table with the 17 lithotypes identified in the Tannwald drill core presented, along with their corresponding sedimentological descriptions and interpretations. Respective core photos are shown in Figs. 3 and 4.

No: *abbreviation* core photo	Lithofacies	Description	Interpretation
1: *B* Fig. 3a	Molasse bedrock	Strongly to moderately consolidated siltstones and sandstones with decimeter-thick marl sequences.	Upper Freshwater Molasse (tOS) as found in the study area in previous drillings (Ellwanger et al., 2011) and seismic survey (Burschil et al., 2018)
2: *Dmm* Fig. 3d, e	Diamict, massive	Matrix-supported and poorly sorted diamict, slightly to very sandy silt matrix (70 %–95 %) and occasional cobbles; angular to rounded components with glacial striations, Alpine and local Molasse clast lithologies	(i) Subglacial traction till (Evans et al., 2006) or (ii) terrestrial or subaqueous cohesive debris flows (Mulder and Alexander, 2001; Eyles et al, 1983)
3: *Dms* Fig. 3f	Diamict, stratified	Matrix-supported to clast-supported and poorly sorted diamict, bedded by centimeter- to decimeter-thick variations in matrix composition and clast size; bedding locally inclined or graded; with slightly to very sandy silt matrix (50 %–95 %) and occasional cobbles; angular to rounded components with glacial striations, Alpine and local Molasse clast lithologies (strongly varying proportions)	Melt-out till (Evans et al., 2006) or proximal hyperconcentrated density flow deposits (Mulder and Alexander, 2001)
4: *Mgt* Fig. 3b, c	Mélange	Consolidated and unconsolidated Molasse sand- and siltstone fragments showing in situ crushing and brecciation.	Deformed bedrock rafts (Benn and Evans, 1996; Hiemstra and van der Meer, 1997)
5: *Mcc* Fig. 4h	Mud-clast conglomerate	Horizontally aligned accumulations of well-sorted fines in a coarser, mostly sandy matrix; often show soft sediment deformation	Reworked fine lacustrine sediments eroded by subaquatic mass movements (e.g., Li et al., 2017)
6: *Gms* Fig. 3g	Gravel, sandy	Clast-supported and moderately sorted gravel with cobbles and fine sandy matrix; massive to crudely bedded; subangular to rounded components, Alpine and Molasse clast lithologies, locally glacial striations (33.09–32.28 m depth).	Distal fluvial to glaciofluvial deposits
7: *Gmf* Fig. 3h	Gravel, silty	Clast-supported and poorly sorted gravel with cobbles and silty coarse sand matrix (prone to coring-induced deformation); massive; subangular to rounded components, Alpine and Molasse clast lithologies	Proximal fluvial to glaciofluvial deposits
8: *Sm*	Sand, massive	Well-sorted fine to medium sand; massive to crudely bedded by localized millimeter- to centimeter-thick variations in silt content and dominant grain-size fraction	Hyperconcentrated density flow deposits (Mulder and Alexander, 2001)

Table A1. Continued.

No: *abbreviation* core photo	Lithofacies	Description	Interpretation
9: *Sh* Fig. 4a, b	Sand, horizontally bedded	Well to moderately sorted fine to medium sand; bedded by centimeter- to decimeter-thick variations in silt content and dominant grain-size fraction, locally with silt and clay laminae	Subaquatic channel fills
10: *Sc* Fig. 4a	Sand, cross-bedded	Well-sorted fine to medium sand; centimeter-thick cross-bedding by silt content and variations in dominant grain-size fraction	Subaquatic channel fills
11: *Sl* Fig. 4h	Sand, laminated	Well-sorted fine to medium sand, laminated (mottled) by varying silt content and dominant grain-size fraction ranging from silty sand up to silt and clay	Proximal turbidity deposits (Bouma, 1962).
12: *Fm* Fig. 4j	Fines, massive	Very well-sorted silt and clay, massive to locally crudely interbedded by fine sand laminae	Suspension settling (Eyles et al., 1993).
13: *Fm(d)* Fig. 4e	Fines, massive, dropstones	Fm with dropstones locally showing glacial striations	Suspension settling in a proglacial lake with ice rafting (Bennett et al., 1996).
14: *Fl* Fig. 4c	Fines, laminated	Very well-sorted clay and silt bedded by millimeter- to centimeter-thick variations in dominant grain-size reflected in slight changes of color	Distal sedimentation of turbidity currents in a proglacial lake (Smith and Ashley, 1985).
15: *Fl(d)* Fig. 4f	Fines, laminated, dropstones	...with dropstones locally showing glacial striations	Distal sedimentation of turbidity currents in a proglacial lake with ice rafting (Bennett et al., 1996)
16: *Flr* Fig. 4d	Fines, laminated, rhythmites	Very well-sorted clay and silt bedded by normal graded laminae and beds with strongly varying thickness (mm to dm thick) of varying dominant grain-size fraction ranging from fine sand to clay	Proximal turbidity deposits (Eyles et al., 1993; Bouma, 1962: Bouma divisions C–E)
17: *Flr(d)* Fig. 4g	Fines, laminated, rhythmites, dropstones	...with dropstones showing glacial striations	Proximal turbidity deposits floating in a proglacial lake with ice rafting (Eyles et al., 1983).

Data availability. The DOVE operational dataset is published under https://doi.org/10.5880/ICDP.5068.001 (DOVE-Phase 1 Scientific Team et al., 2023b) together with the operational report (https://doi.org/10.48440/ICDP.5068.001, DOVE-Phase 1 Scientific Team et al., 2023a) and the explanatory remarks (https://doi.org/10.48440/ICDP.5068.002, DOVE-Phase 1 Scientific Team et al., 2023c). Furthermore, the dataset is accessible via the ICDP website: https://www.icdp-online.org/projects/by-continent/europe/dove-switzerland/ (ICDP, 2024). Information on the project and the data is also available on the ICDP DOVE project website: https://www.icdp-online.org/projects/by-continent/europe/dove-switzerland (DOVE-Phase 1 Scientific Team, 2024).

Author contributions. FP and FSA played a pivotal role in conceptualizing the research project, project management, and coordination. BS and DT were drill site geologists, and BS performed the ICD. SS performed the data preprocessing and preparation. LG, MWB, and UWS provided valuable insights into the theoretical framework and methodology used in this study. Their guidance significantly influenced the research approach. All authors contributed to the writing of the manuscript and editing process.

Competing interests. The contact author has declared that none of the authors has any competing interests.

Disclaimer. Publisher's note: Copernicus Publications remains neutral with regard to jurisdictional claims made in the text, published maps, institutional affiliations, or any other geographical representation in this paper. While Copernicus Publications makes every effort to include appropriate place names, the final responsibility lies with the authors.

Acknowledgements. We would like to express gratitude to the International Scientific Continental Drilling Program (ICDP) for their support during drilling and for providing access to the online database "mDIS". Special thanks to the drilling firm "H. Anger's Söhne", particularly Mirko Huber and the dedicated drilling crew, including Jürgen Pröhl, Markus Schiek, J. Achler, Mohammad Alhamad, Hsaan Alsasihl, Asabdi, Peter Goor, Frank Hapke, Zoltan Mihalti, Zoltan Olah, Jens Täubert, Lutz Tonne, and Peter Toth, who skillfully navigated challenging sedimentary conditions and provided essential on-site infrastructure. We highly appreciate the cooperation of the local authorities of the municipality of Ingoldingen in the district of Biberach, particularly Roland Wersch, Jürgen Schell, and Reiner Traub. Their support for the drilling project and granting access to refrigerated rooms was instrumental. Thanks are due to the Leibniz Institute for Applied Geophysics (LIAG) for their crucial involvement in the project, including the pre-drilling seismic survey and downhole logging in all three holes. In particular, we thank Thomas Burschil and Hermann Buness for providing important seismic data. LIAG's contribution of technical infrastructure for scientific operations on site, as well as outreach efforts to schools and local events, is appreciated. We would also like to thank Merlin Kamke for documenting our work through photography. Special recognition goes to Julijana Gajic, Patrizia Ruffiner, and Aaron Alexander Hutter for their efforts in processing and analyzing the TIC and TOC samples. Lastly, my gratitude to the entire DOVE science team for their collaborative contributions that have enriched the research experience and contributed to the project's success. We thank the two reviewers and the editors for constructive reviews.

Financial support. This research has been funded by the ICDP, the Deutsche Forschungsgemeinschaft (DFG, grant nos. KR2073/3-1, BU 2467/1-2, GA749/5-1, BU2467/3-1, BU 3894/2-1, BU3894/3-1, and PR 957/6-1), Nagra, ENSI, LGRB, LFU, LIAG, BOKU Vienna, University of Freiburg, and the University of Bern.

Review statement. This paper was edited by Nadine Hallmann and reviewed by two anonymous referees.

References

Alley, R. B., Cuffey, K. M., Evenson, E. B., Strasser, J. C., Lawson, D. E., and Larson, G. J.: How glaciers entrain and transport basal sediment: physical constraints, Quaternary Sci. Rev., 16, 1017–1038, 1997.

Alley, R. B., Cuffey, K. M., and Zoet, L. K.: Glacial erosion: status and outlook, Ann. Glaciol., 60, 1–13, https://doi.org/10.1017/aog.2019.38, 2019.

Anselmetti, F. S., Drescher-Schneider, R., Furrer, H., Graf, H. R., Lowick, S. E., Preusser, F., and Riedi, M. A.: A 180,000 years sedimentation history of a peri-Alpine overdeepened glacial trough (Wehntal, N-Switzerland), Swiss J. Geosci., 103, 345–361, https://doi.org/10.1007/s00015-010-0041-1, 2010.

Anselmetti, F. S., Bavec, M., Crouzet, C., Fiebig, M., Gabriel, G., Preusser, F., Ravazzi, C., and DOVE scientific team: Drilling Overdeepened Alpine Valleys (ICDP-DOVE): quantifying the age, extent, and environmental impact of Alpine glaciations, Sci. Dril., 31, 51–70, https://doi.org/10.5194/sd-31-51-2022, 2022.

Bachmann, G. H., Müller, M., and Weggen, K.: Evolution of the molasse basin (Germany, Switzerland), Tectonophysics, 137, 77–92, https://doi.org/10.1016/0040-1951(87)90315-5, 1987.

Benn, D. I. and Evans, D. J.: The interpretation and classification of subglacially-deformed materials, Quaternary Sci. Rev., 15, 23–52, https://doi.org/10.1016/0277-3791(95)00082-8, 1996.

Bennett, M. R., Doyle, P., and Mather, A. E.: Dropstones: their origin and significance, Palaeogeogr. Palaeocl., 121, 331–339, https://doi.org/10.1016/0031-0182(95)00071-2, 1996.

Bouma, A. H.: Sedimentology of some Flysch deposits: a graphic approach to facies interpretation, Elsevier, Amsterdam, the Netherlands, https://lib.ugent.be/catalog/rug01:000978747 (last access: 12 December 2023), 1962.

Buechi, M. W., Frank, S. M., Graf, H. R., Menzies, J., and Anselmetti, F. S.: Subglacial emplacement of tills and meltwater deposits at the base of overdeepened bedrock troughs, Sedimentology, 64, 658–685, https://doi.org/10.1111/sed.12319, 2017.

Buechi, M. W., Graf, H. R., Haldimann, P., Lowick, S. E., and Anselmetti, F. S.: Multiple Quaternary erosion and infill cycles in overdeepened basins of the northern Alpine foreland, Swiss

J. Geosci., 111, 133–167, https://doi.org/10.1007/s00015-017-0289-9, 2018.

Burschil, T., Buness, H., Tanner, D. C., Wielandt-Schuster, U., Ellwanger, D., and Gabriel, G.: High-resolution reflection seismics reveal the structure and the evolution of the Quaternary glacial Tannwald Basin, Near Surf. Geophys., 16, 593–610, 2018.

Buness, H., Burschil, T., and Tanner, D. C.: Imaging glacial sediments and tectonics with a small-scale 3-D reflection seismic survey, 26th European Meeting of Environmental and Engineering Geophysics, 7–8 December 2020, online, 1, 1–4, https://doi.org/10.3997/2214-4609.202020094, 2020.

Buness, H., Tanner, D. C., Burschil, T., Gabriel, G., and Wielandt-Schuster, U.: Cuspate-lobate folding in glacial sediments revealed by a small-scale 3-D seismic survey, J. Appl. Geophy., 200, 104614, https://doi.org/10.1016/j.jappgeo.2022.104614, 2022.

Cook, S. J. and Swift, D. A.: Subglacial basins: Their origin and importance in glacial systems and landscapes, Earth-Sci. Rev., 115, 332–372, https://doi.org/10.1016/j.earscirev.2012.09.009, 2012.

Dehnert, A., Lowick, S. E., Preusser, F., Anselmetti, F. S., Drescher-Schneider, R., Graf, H. R., Heller, F., Horstmeyer, H., Kemna, H. A., Nowaczyk, N. R., Züger, A., and Furrer, H.: Evolution of an overdeepened trough in the northern Alpine Foreland at Niederweningen, Switzerland, Quaternary Sci. Rev., 34, 127–145, https://doi.org/10.1016/j.quascirev.2011.12.015, 2012.

Doppler, G., Kroemer, E., Rögner, K., Wallner, J., Jerz, H., and Grottenthaler, W.: Quaternary stratigraphy of southern Bavaria, EandG Quaternary Sci. J., 60, 23, https://doi.org/10.3285/eg.60.2-3.08, 2011.

DOVE-Phase 1 Scientific Team, Anselmetti, F. S., Beraus, S., Buechi, M. W., Buness, H., Burschil, T., Fiebig, M., Firla, G., Gabriel, G., Gegg, L., Grelle, T., Heeschen, K., Kroemer, E., Lehne, C., Lüthgens, C., Neuhuber, S., Preusser, F., Schaller, S., Schmalfuss, C., Schuster, B., Tanner, D. C., Thomas, C., Tomonaga, Y., Wieland-Schuster, U., and Wonik, T.: Drilling Overdeepened Alpine Valleys (DOVE) – Operational Report of Phase 1, (ICDP Operational Report), GFZ German Research Centre for Geosciences, Potsdam, 70 pp., https://doi.org/10.48440/ICDP.5068.001, 2023a.

DOVE-Phase 1 Scientific Team, Anselmetti, F. S., Beraus, S., Buechi, M. W., Buness, H., Burschil, T., Fiebig, M., Firla, G., Gabriel, G., Gegg, L., Grelle, T., Heeschen, K., Kroemer, E., Lehne, C., Lüthgens, C., Neuhuber, S., Preusser, F., Schaller, S., Schmalfuss, C., Schuster, B., Tanner, D. C., Thomas, C., Tomonaga, Y., Wieland-Schuster, U., and Wonik, T.: Drilling Overdeepened Alpine Valleys (DOVE) – Operational Dataset of DOVE Phase 1, GFZ Data Services [data set], https://doi.org/10.5880/ICDP.5068.001, 2023b.

DOVE-Phase 1 Scientific Team, Anselmetti, F. S., Beraus, S., Buechi, M. W., Buness, H., Burschil, T., Fiebig, M., Firla, G., Gabriel, G., Gegg, L., Grelle, T., Heeschen, K., Kroemer, E., Lehne, C., Lüthgens, C., Neuhuber, S., Preusser, F., Schaller, S., Schmalfuss, C., Schuster, B., Tanner, D. C., Thomas, C., Tomonaga, Y., Wieland-Schuster, U., and Wonik, T.: Drilling Overdeepened Alpine Valleys (DOVE) – Explanatory remarks on the operational dataset, ICDP Operational Dataset – Explanatory Remarks, GFZ German Research Centre for Geosciences [data set], Potsdam, 34 pp., https://doi.org/10.48440/ICDP.5068.002, 2023c.

DOVE-Phase 1 Scientific Team: DOVE – What is DOVE?, https://www.dove-icdp.eu/ (last access: 26 June 2024), 2024.

Dürst Stucki, M. and Schlunegger, F.: Identification of erosional mechanisms during past glaciations based on a bedrock surface model of the central European Alps, Earth Planet. Sc. Lett., 384, 57–70, https://doi.org/10.1016/j.epsl.2013.10.009, 2013.

Dürst Stucki, M., Reber, R., and Schlunegger, F.: Subglacial tunnel valleys in the Alpine Foreland: an example from Bern, Switzerland, Swiss J. Geosci., 103, 363–374, https://doi.org/10.1007/s00015-010-0042-0, 2010.

Ellwanger, D.: Lithostratigraphische Entwicklung des baden-württembergischen Rheingletschergebietes: übertiefte Becken- und Moränenlandschaft, LGRB-Fachbericht 2015/4a & 4b, Landesamt für Geologie, Rohstoffe und Bergbau (RP Freiburg, Baden-Württemberg), 2015.

Ellwanger, D., Bibus, E., Bludau, W., Kösel, M., and Merkt, J.: Baden-Württemberg, in: Das Quartär Deutschlands: 255–295, edited by: Benda, L., Berlin, Stuttgart, New York, https://www.schweizerbart.de/publications/detail/artno/001199531 (last access: 12 December 2023), 1995.

Ellwanger, D., Wielandt-Schuster, U., Franz, M., and Simon, T.: The Quaternary of the southwest German Alpine Foreland (Bodensee-Oberschwaben, Baden-Württemberg, Southwest Germany), EandG Quaternary Sci. J., 60, 22, https://doi.org/10.3285/eg.60.2-3.07, 2011.

Evans, D. J. A., Phillips, E. R., Hiemstra, J. F., and Auton, C. A.: Subglacial till: Formation, sedimentary characteristics and classification, Earth-Sci. Rev., 78, 115–176, https://doi.org/10.1016/j.earscirev.2006.04.001, 2006.

Eyles, C. H., Eyles, N., and França, A. B.: Glaciation and tectonics in an active intracratonic basin: the Late Palaeozoic Itararé Group, Paraná Basin, Brazil, Sedimentology, 40, 1–25, https://doi.org/10.1111/j.1365-3091.1993.tb01087.x, 1993.

Eyles, N., Eyles, C. H., and Miall, A. D.: Lithofacies types and vertical profile models; an alternative approach to the description and environmental interpretation of glacial diamict and diamictite sequences, Sedimentology, 30, 393–410, https://doi.org/10.1111/j.1365-3091.1983.tb00679.x, 1983.

Fernandes, M., Oliva, M., and Vieira, G.: Paraglacial slope failures in the Aran valley (Central Pyrenees), Quaternary Int., 566, 24–38, https://doi.org/10.1016/j.quaint.2020.07.045, 2020.

Fiebig, M.: Pleistozäne Ablagerungen im süddeutschen und im neuseeländischen Alpenvorland – ein Vergleich, Doctoral dissertation, Albert-Ludwigs-Universität Freiburg im Breisgau, 122 pp., https://freidok.uni-freiburg.de/inst/2040 (last access: 12 December 2023), 1995.

Fiebig, M., Herbst, P., Drescher-Schneider, R., Lüthgens, C., Lomax, J., and Doppler, G.: Some remarks about a new Last Glacial record from the western Salzach foreland glacier basin (Southern Germany), Quaternary Int., 328–329, 107–119, https://doi.org/10.1016/j.quaint.2013.12.048, 2014.

Fischer, H.: Excess K-Ar ages of glauconite from the Upper Marine Molasse and evidence for glauconitization of mica, Geol. Rundsch., 76, 885–902, 1987.

Gegg, L. and Preusser, F.: Comparison of overdeepened structures in formerly glaciated areas of the northern Alpine foreland and northern central Europe, E&G Quaternary Sci. J., 72, 23–36, https://doi.org/10.5194/egqsj-72-23-2023, 2023.

Gegg, L., Deplazes, G., Keller, L., Madritsch, H., Spillmann, T., Anselmetti, F. S., and Buechi, M. W.: 3D morphology of a glacially overdeepened trough controlled by underlying bedrock geology, Geomorphology, 394, 107950, https://doi.org/10.1016/j.geomorph.2021.107950, 2021.

Geyer, O. F., Gwinner, M. P., Geyer, M., Nitsch, E., and Simon, T.: Geologie von Baden-Württemberg, Schweizerbart, 117–118, https://scholar.archive.org/work/5g5oa6bb5jdl3mztto7wpiv3bi/access/wayback/https://journals.wlb-stuttgart.de/ojs/index.php/sh/article/download/2880/2924 (last access: 12 December 2023), 2011.

Graf, H. R.: Stratigraphie von Mittel- und Spätpleistozän in der Nordschweiz. Beiträge zur Geologischen Karte der Schweiz (N.F.), 168, Landesgeologie, Swisstopo, 198 pp., https://doi.org/10.3285/eg.58.1.02, 2009.

Hahne, J., Ellwanger, D., Franz, M., Stritzke, R., and Wielandt-Schuster, U.: Pollenanalytische Untersuchungsergebnisse aus dem baden-württembergischen Rheinsystem Oberrheingraben, Hochrhein, Oberschwaben – eine Zusammenfassung des aktuellen Kenntnisstandes, LGRB Info, 26, 119–154, https://produkte.lgrb-bw.de/docPool/c618_data.pdf (last access: 12 December 2023), 2012.

Hiemstra, J. F. and van der Meer, J. J. M.: Pore-water controlled grain fracturing as an indicator for subglacial shearing in tills, J. Glaciol., 43, 446–454, https://doi.org/10.3189/S0022143000035036, 1997.

Huuse, M. and Lykke-Andersen, H.: Overdeepened Quaternary valleys in the eastern Danish North Sea: morphology and origin, Quaternary Sci. Rev., 19, 1233–1253, https://doi.org/10.1016/S0277-3791(99)00103-1, 2000.

ICDP: Drilling Overdeepened Alpine Valleys, https://www.icdp-online.org/projects/by-continent/europe/dove-switzerland/ (last access: 26 June 2024), 2024.

Lämmermann-Barthel, J., Neeb, I., Hinderer, M., Ellwanger, D., and Frechen, M.: Sediment budget of Pliocene and Quaternary unconsolidated deposits of the Rhine Glacier area, Swiss Midlands and the Upper Rhine Graben, in: EGS-AGU-EUG Joint Assembly, 13554, https://www.researchgate.net/profile/Inge-Neeb/publication (last access: 12 December 2023), 2003.

Lawson, D. E.: Mobilization, movement and deposition of active subaerial sediment flows, Matanuska Glacier, Alaska, J. Geol., 90, 279–300, https://doi.org/10.1086/628680, 1982.

Li, S., Li, S., Shan, X., Gong, C., and Yu, X.: Classification, formation, and transport mechanisms of mud clasts, Int. Geol. Rev., 59, 1609–1620, https://doi.org/10.1080/00206814.2017.1287014, 2017.

Menzies, J.: Subglacial hydraulic conditions and their possible impact upon subglacial bed formation, Sediment. Geol., 62, 125–150, https://doi.org/10.1016/0037-0738(89)90112-7, 1989.

Meyers, P. A. and Teranes, J. L.: Sediment Organic Matter, in: Tracking Environmental Change Using Lake Sediments: Physical and Geochemical Methods, edited by: Last, W. M. and Smol, J. P., Springer Netherlands, Dordrecht, 239–269, https://doi.org/10.1007/0-306-47670-3_9, 2001.

Mulder, T. and Alexander, J.: The physical character of subaqueous sedimentary density flows and their deposits, Sedimentology, 48, 269–299, https://doi.org/10.1046/j.1365-3091.2001.00360.x, 2001.

O'Regan, M., Jakobsson, M., and Kirchner, N.: Glacial geological implications of overconsolidated sediments on the Lomonosov Ridge and Yermak Plateau, Quaternary Sci. Rev., 29, 3532–3544, https://doi.org/10.1016/j.quascirev.2010.09.009, 2010.

Pomper, J., Salcher, B. C., Eichkitz, C., Prasicek, G., Lang, A., Lindner, M., and Götz, J.: The glacially overdeepened trough of the Salzach Valley, Austria: Bedrock geometry and sedimentary fill of a major Alpine subglacial basin, Geomorphology, 295, 147–158, https://doi.org/10.1016/j.geomorph.2017.07.009, 2017.

Preusser, F., Drescher-Schneider, R., Fiebig, M., and Schlüchter, C.: Re-interpretation of the Meikirch pollen record, Swiss Alpine Foreland, and implications for Middle Pleistocene chronostratigraphy, J. Quaternary Sci., 20, 607–620, https://doi.org/10.1002/jqs.930, 2005.

Preusser, F., Reitner, J. M., and Schlüchter, C.: Distribution, geometry, age and origin of overdeepened valleys and basins in the Alps and their foreland, Swiss J. Geosci., 103, 407–426, https://doi.org/10.1007/s00015-010-0044-y, 2010.

Preusser, F., Graf, H. R., Keller, O., Krayss, E., and Schlüchter, C.: Quaternary glaciation history of northern Switzerland, E&G Quaternary Sci. J., 60, 21, https://doi.org/10.3285/eg.60.2-3.06, 2011.

Ravier, E., Buoncristiani, J. F., Clerc, S., Guiraud, M., Menzies, J., and Portier, E.: Sedimentological and deformational criteria for discriminating subglaciofluvial deposits from subaqueous ice-contact fan deposits, A Pleistocene example (Ireland), Sedimentology, 61, 1382–1410, https://doi.org/10.1111/sed.12111, 2014.

Schaller, S., Buechi, M. W., Schuster, B., and Anselmetti, F. S.: Drilling into a deep buried valley (ICDP DOVE): a 252 m long sediment succession from a glacial overdeepening in northwestern Switzerland, Sci. Dril., 32, 27–42, https://doi.org/10.5194/sd-32-27-2023, 2023.

Schlüchter, C.: The most complete Quaternary record of the Swiss Alpine Foreland, Palaeogeogr. Palaeocl., 72, 141–146, https://doi.org/10.1016/0031-0182(89)90138-7, 1989.

Schuster, B., Amschwand, D., Huber, M. L., Madritsch, H., Deplazes, G., and Büchi, M.: Quaternary Borehole QBO Kleinandelfingen-Laubhau (QKLA), Data Rep., https://boris.unibe.ch/id/eprint/167486 (last access: 12 December 2023), 2020.

Schwenk, M. A., Schläfli, P., Bandou, D., Gribenski, N., Douillet, G. A., and Schlunegger, F.: From glacial erosion to basin overfill: a 240 m-thick overdeepening–fill sequence in Bern, Switzerland, Sci. Dril., 30, 17–42, https://doi.org/10.5194/sd-30-17-2022, 2022.

Siegenthaler, C. and Huggenberger, P.: Pleistocene Rhine gravel: deposits of a braided river system with dominant pool preservation, Geol. Soc., London, Special Publications, 75, 147–162, 1993.

Smith, N. D. and Ashley, G. M.: Proglacial lacustrine environments, in: Glacial Sedimentary Environments, edited by: Ashley, G. M., Shaw, J., and Smith, N. D., SEPM Short, 16, 135–215, 1985.

Visser, J. N. J., Colliston, W. P., and Terblanche, J. C.: The origin of soft-sediment deformation structures in Permo-Carboniferous glacial and proglacial beds, South Africa, J. Sediment. Res., 54, 1183–1196, https://doi.org/10.1306/212F8594-2B24-11D7-8648000102C1865D, 1984.